

5 Gbps Optical Wireless Communication using Commercial SPAD Array Receivers

Shenjie Huang, Cheng Chen, Rui Bian, Harald Haas, *Fellow, IEEE*, and Majid Safari, *Senior Member, IEEE*

Abstract—Photon counting detectors such as single-photon avalanche diode (SPAD) arrays can be utilized to improve the sensitivity of optical wireless communication (OWC) systems. However, the achievable data rate of SPAD-based OWC systems is strongly limited by the nonlinearity induced by SPAD dead time. In this work, the performances of SPAD receivers for two different modulation schemes, namely, on-off keying (OOK) and orthogonal frequency division multiplexing (OFDM), are compared demonstrating contrasting optimal regimes of operation. We employ nonlinear equalization and peak-to-average power ratio optimization by adjusting the OFDM clipping level to achieve record experimental data rates of up to 5 Gbps. In particular, the experimental results demonstrate the achievable data rates of 3.22 Gbps and 5 Gbps when OOK and OFDM are employed, respectively, at a BER target of 2×10^{-3} . It is also illustrated that to achieve the best data rate performance over a wide range of received power, adaptive switching between OOK and OFDM may be utilized.

Index Terms—Optical wireless communication, single-photon avalanche diode, dead time.

I. INTRODUCTION

Due to the scarcity of the radio frequency, optical wireless communication (OWC) has attracted significant interest in both industry and scientific community in recent years. Compared to traditional radio frequency (RF) communication, the potential advantages of OWC mainly include high data rates, excellent security levels and license-free spectrum [1]. The performance of OWC systems can be significantly degraded by occasional outages caused by received optical power fluctuations. One effective method to mitigate this performance degradation is employing single-photon avalanche diode (SPAD) based receivers. Photon counting capability of SPADs can be achieved by biasing the traditional photodiode above the breakdown voltage and operating it in the Geiger mode. SPAD has much higher sensitivity compared to the linear photodiode, e.g., P-i-N photodiode (PIN PD) and avalanche photodiode (APD) [2]. However, after an avalanche triggered by a photon detection, the SPAD needs to be quenched and becomes blind to any incident photon arrivals for a short period of time called dead time. It is known that SPAD receivers suffer from dead-time-induced nonlinear effects including nonlinear distribution [3] and intersymbol interference [4].

Shenjie Huang and Majid Safari are with the School of Engineering, the University of Edinburgh, Edinburgh EH9 3JL, U.K. (e-mail: {shenjie.huang, majid.safari}@ed.ac.uk).

Cheng Chen and Harald Haas are with LiFi Research and Development Centre, University of Strathclyde, Glasgow G1 1RD, U.K. (e-mail: {c.chen, harald.haas}@strath.ac.uk)

Rui Bian is with pureLiFi, Edinburgh EH12 5EZ, U.K. (e-mail: rui.bian@purelifi.com).

In the literature, many works have been conducted to improve the data rate of SPAD-based receivers. For example, in [4] a novel detection scheme for SPAD-based systems is proposed in which the information of both photon counts and photon arrival times are utilised to realize the optimal detection. In addition, by using decision feedback (DFE) equalizer, gigabit communication using commercial SPAD receivers with OOK modulation is experimentally demonstrated [5], [6]. This work aims to further explore the achievable data rate of the commercial SPAD receivers. In this work, for the first time, the nonlinear equalizer based on Volterra series model is employed to mitigate the nonlinear effects of SPAD receivers. The superiority of the nonlinear equalization over the traditional equalization is demonstrated. In addition, besides OOK modulation, the application of OFDM in SPAD-based OWC systems is investigated in which the optimization of peak-to-average power ratio (PAPR) by controlling OFDM clipping level is further adopted to reduce the receiver nonlinearity degradation. The experimental results present the effectiveness of the employed techniques on the achievable data rate improvement.

This paper is organized as follows. The characteristics of the employed commercial SPAD receiver are discussed in Section II. The experimental setup is described in Section III. The data transmission with OOK and OFDM are demonstrated in Section IV and Section V, respectively. Finally, we conclude this work in Section VI.

II. SPAD ARRAY RECEIVER

The commercial SPAD receiver (also known as silicon photomultiplier, SiPM) employed in this work is On Semiconductor J-30020 with $N_{\text{SPAD}} = 14410$ SPAD pixels or microcells. The total area of the detector is $3.07 \times 3.07 \text{ mm}^2$ and the fill factor is 62% [7]. The detected photon rate of the employed SPAD receiver can be approximated as

$$C = \frac{P_R \Upsilon_{\text{PDE}} / h\nu}{1 + P_R \Upsilon_{\text{PDE}} T_d / N_{\text{SPAD}} h\nu}, \quad (1)$$

where P_R denotes the received signal power, Υ_{PDE} is the photon detection efficiency (PDE), h is Planck's constant, ν is light frequency, and T_d is the dead time which is around 66 ns [8]. It is presented in (1) that the detected photon rate of the employed SPAD receiver has an approximately linear relationship with incident photon rate (or equivalently P_R) in low incident power regime, but as the incident power increases, the photocurrent becomes nonlinear and finally saturates at a fixed value $C_{\text{max}} = N_{\text{SPAD}} / T_d$ [6]. Note that although the considered SPAD receiver is passive quenched, due to its

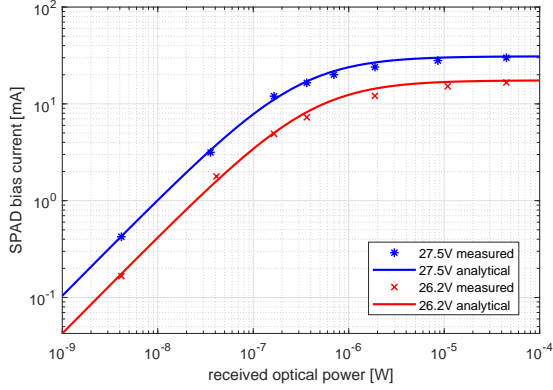


Fig. 1. The SPAD bias current versus the received optical power under various bias voltages.

quasi-analog output, its response is different from that of the passive quenched SPAD receiver with digital output and is, in fact, similar to that of the active quenched SPAD receiver with digital output [9].

After a microcell detects a photon, it has to be recharged during the dead time. Denoting Q as the charge needed for the microcell to get back to its original voltage, the current needed to maintain the operational bias voltage of the receiver is given by [6]

$$I_{\text{bias}} = QC = \frac{QP_R\Upsilon_{\text{PDE}}/h\nu}{1 + P_R\Upsilon_{\text{PDE}}T_d/N_{\text{SPAD}}h\nu}. \quad (2)$$

As this bias current is proportional to the detected photon rate, one can use it to evaluate the saturation effect of the SPAD receiver. Fig. 1 presents two examples of the measured bias current versus the received optical power under various bias voltages. It is demonstrated that the measured bias current matches with that of the analytical expression given in (2). Note that the parameters Q and Υ_{PDE} vary with the bias voltage. In particular, when bias voltages is 27.5 V, the parameters $Q = 0.14$ pC and $\Upsilon_{\text{PDE}} = 0.36$ are employed to achieve the analytical result which are close to the values selected in [6]. The nonlinear response of the SPAD receiver can be clearly observed in Fig. 1. Such nonlinearity can significantly degrade the communication performance. It is also presented that larger bias voltage results in higher current because of the higher SPAD gain and PDE. This is, however, at the expense of higher dark count rate (DCR) and severer microcell crosstalk. Our measurements show that the performance achieved with 27.5 V bias voltage is superior to that of the other voltages. Therefore, in the following demonstration the bias voltage 27.5 V is employed.

III. EXPERIMENT SETUP

Fig. 2 presents the block diagram of the experimental setup. The demonstration is operated in dark condition. At the transmitter side, the binary data stream is firstly generated using MATLAB in PC. After applying the modulation (OOK or DCO-OFDM) and root-raised-cosine (RRC) pulse-shaping, the modulated discrete signal with desired sampling rate is sent to arbitrary waveform generator (AWG, Keysight M8195A) to

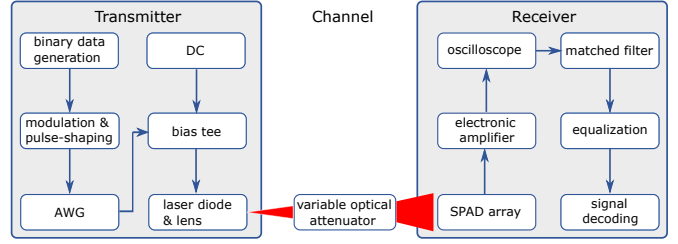


Fig. 2. The schematic diagram of the experimental setup.

be converted to the analog waveform. The employed AWG has a sampling rate 16 GSa/s and a resolution of the digital-to-analog (DAC) unit 8 bits. The output AC signal of the AWG is then combined with the DC bias from a power supply (Keysight E36313A) by utilizing a bias tee (Mini-Circuits ZFBT-6GW+). The output signal of the bias tee is used to drive the laser diode (Thorlabs L405P20) which has a central wavelength of 405 nm. This laser diode is employed as its central wavelength is close to the peak PDE wavelength of the SPAD receiver, i.e., 420 nm. In the demonstration, the bias voltage of the laser diode and the Vpp of the modulated electrical signal are set to 4.55 V and 0.8 V, respectively. Finally, an aspheric lens (Thorlabs 354330-A) is used to collimate the laser beam.

For OWC systems, the received optical power normally changes over time due to various channel effects, e.g., scintillation in FSO [1] and random orientation in VLC [10]. In order to emulate the optical power fluctuation introduced by practical OWC channels, a variable optical attenuator is used which comprises a neutral density filter wheel (Thorlabs FW1A) and a wire grid polarizing film (Edmund optics 34254). By rotating the filter wheel and the polariser, the continuous change of the channel path loss and hence the received signal power can be achieved. Note that changing the channel path loss can change not only the received DC optical signal but also the AC one proportionally.

The laser beam after propagating through the attenuator illuminates the SPAD array receiver. To avoid the excessive received optical power which might damage the SPAD array, the laser beam is diffracted so that the beam size on the receiver plane is much larger than the SPAD sensor area. The fast output of the SPAD receiver is amplified by the electronic amplifier (Mini-Circuits ZX60-43-S+) and then fed to the oscilloscope (Keysight DSA90804A) which has a bandwidth of 8 GHz. The received waveform captured by the oscilloscope is sent to the PC for the offline processing. The matched filtering which matches with the signal pulse is applied and the output downsampled signal then goes through specific equalizer which varies with the investigated system. Finally, after equalization the signal decoding process is adopted to recover the transmitted information bits.

IV. EFFICIENT DATA TRANSMISSION WITH OOK

In this work, we consider two commonly used modulation schemes, i.e., OOK and DC-biased optical OFDM (DCO-OFDM). For the system with OOK, two different equalization methods are considered at the receiver, i.e., linear

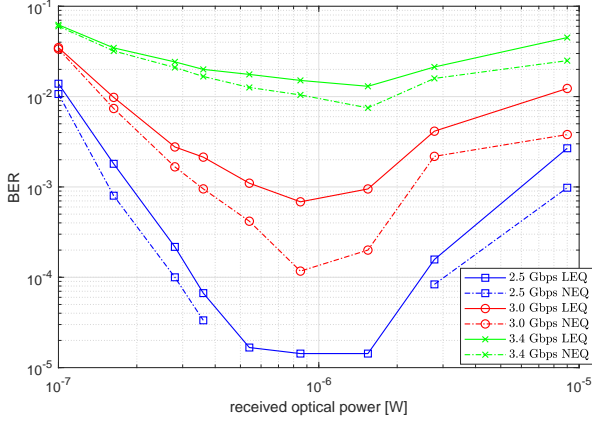


Fig. 3. The BER versus the received optical power under various data rates in the presence of linear equalization (LEQ) or nonlinear equalization (NEQ) when OOK modulation is employed.

and nonlinear equalization. In both equalization methods, the recursive least square (RLS) algorithm is utilized to train the tap weights. As the dead-time-induced effects are inherently nonlinear, it is expected that nonlinear equalization can result in superior performance compared to that of linear equalization. The employed nonlinear equalizer is designed based on Volterra series model. Considering the complexity of the higher-order Volterra filter, only the first two orders of the Volterra series are considered. The output of the nonlinear equalizer can be expressed as $d(n) =$

$$\sum_{i=0}^{N_l-1} w_1(i)x(n-i) + \sum_{m_1=0}^{N_{nl}-1} \sum_{m_2=m_1}^{N_{nl}-1} w_2(m_1, m_2)x(n-m_1)x(n-m_2), \quad (3)$$

where $x(n)$ denotes the signal before equalization, N_l and N_{nl} refer to the memory length of the first and second order terms, respectively, and w_1 and w_2 are the corresponding tap weights. In this demonstration, in order to balance the complexity and performance, the memory lengths of the nonlinear equalizer are set to $N_l = 41$ and $N_{nl} = 21$, respectively.

Fig. 3 presents the measured BER versus the received optical power when OOK modulation is employed. It is shown that higher data rate can result in worse BER performance, as expected due to larger ISI effects. The superiority of nonlinear equalizer over its linear counterpart can also be clearly observed. In addition, it is demonstrated that with the increase of the received optical power the BER firstly decreases and then increases. For instance, at a data rate of 3 Gbps, the BER decreases from 0.03 to 10^{-4} when the received optical power increases from $0.1 \mu\text{W}$ to $0.9 \mu\text{W}$, but the BER rises to 2×10^{-3} when the received power increases to $2.8 \mu\text{W}$. This is because in low received power regime, the system is signal power limited and hence increase the signal power can improve the BER performance; however, with the increase of signal power, the dead-time-induced nonlinear distortion and ISI effects come into effect which in turn degrade the performance. Similar BER behaviour has also been reported in many theoretical works [3], [4], [11].

Fig. 4 presents the BER versus the data rate under various

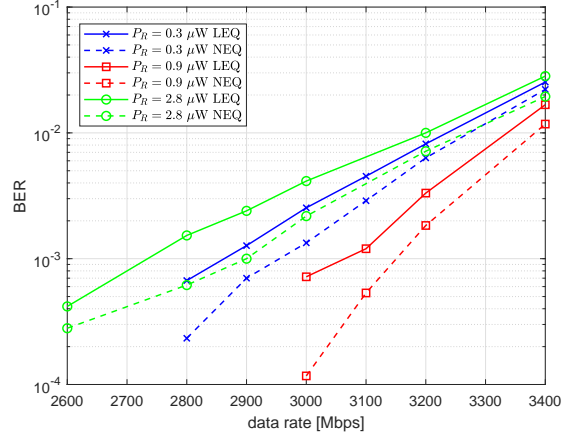


Fig. 4. The BER versus the data rate under various received optical power P_R when OOK modulation is employed. LEQ: linear equalization; NEQ: nonlinear equalization.

received optical power. One can observe that for a specific BER target nonlinear equalizer can provide higher data rate than that of linear equalizer. For instance, when $P_R = 2.8 \mu\text{W}$, with a BER target of 2×10^{-3} the achievable data rate when linear equalizer is employed is 2860 Mbps but the corresponding data rate when nonlinear equalizer is employed increases to 2990 Mbps. In addition, it is again presented that larger P_R does not necessarily result in better performance due to the SPAD nonlinearity. Based on Fig. 4, for any BER target the achievable data rate versus the received power results can also be achieved, as presented later in Fig. 7.

V. DATA TRANSMISSION WITH OFDM

In general, OFDM modulation can be employed to improve the spectral efficiency. The current highest reported data rate achieved by SPAD receiver with OFDM is only 350 Mbps [12] which is much less than the reported achievable data rates when OOK is utilized [6]. In this section, we aim to explore the potential of using OFDM in SPAD-based OWC systems. Two different DCO-OFDM-based systems are considered in this work. The first is the traditional one with single tap frequency domain equalization [13]. For the second system the time-domain nonlinear equalization shown in (3) is further employed to mitigate the nonlinear effects. The nonlinear equalizer at the receiver is applied to the signal after matched filtering and before the Fourier transform operation. The same memory lengths of nonlinear equalizer as OOK transmission are employed. We consider that for both OFDM systems the modulation bandwidth is 1400 MHz and the number of subcarriers is 1024. OFDM enables the use of the adaptive power allocation and bit loading algorithm [14] to improve the achievable data rate which is also adopted in the considered systems.

The time-domain OFDM signal is approximately normal distribution which has high PAPR [15]; however, in practical communication systems with limited dynamic range, this will lead to a significant decrease in transmitted signal power. Therefore, signal clipping is crucial for OFDM transmission.

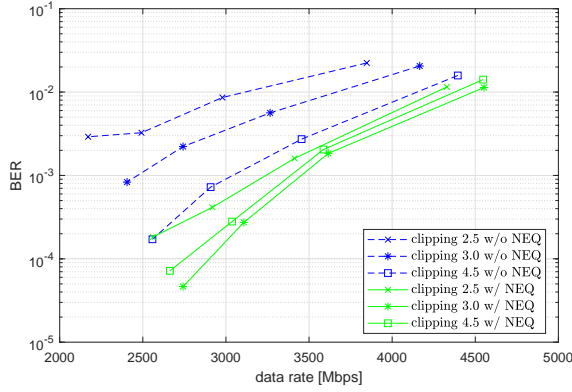


Fig. 5. The BER of OFDM versus the data rate under various clipping levels when the received signal power is $2.8 \mu\text{W}$. NEQ: nonlinear equalization.

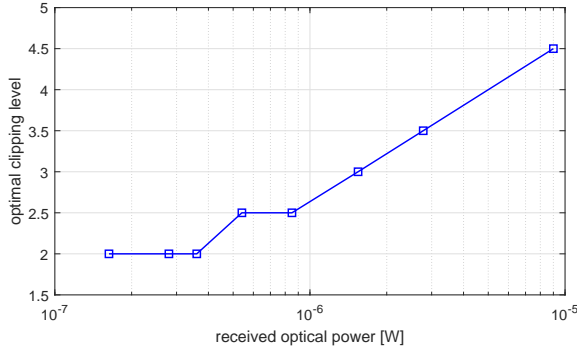


Fig. 6. The optimal clipping level for OFDM versus the received signal power in the presence of nonlinear equalization.

In the proposed systems, a normalized OFDM signal with standard normal distribution in time domain is firstly generated. The signal is then clipped so that the maximal and minimal amplitude are ε and $-\varepsilon$, respectively, where ε denotes the normalised clipping level. Later, the normalized electrical signal is scaled to a desired V_{pp} to drive the laser diode, which is 0.8 V in the proposed systems. The change of ε is equivalent to the change of the PAPR of the transmitted OFDM signal. By selecting larger ε , it is expected that the received optical signal can occupy less dynamic range of the receiver and hence the effect of SPAD nonlinear distortion can be reduced. In addition, choosing larger clipping level can reduce the clipping distortion. However, since the V_{pp} of the transmitted signal is fixed, larger clipping level also results in less signal power which in turn degrades the performance [13]. Therefore, it is expected that the clipping level, or equivalently the PAPR, of the transmitted OFDM signal can be optimized to achieve the best performance.

Fig. 5 presents the BER of the OFDM transmission versus the data rate with various normalized clipping levels in the presence and absence of nonlinear equalization. The superiority of the system with nonlinear equalizer over that without nonlinear equalizer can be clearly observed. In addition, it is demonstrated that the system performance varies with the employed clipping level due to aforementioned trade-off, especially for the system without nonlinear equalizer because of the stronger nonlinear effects. For example, in the absence

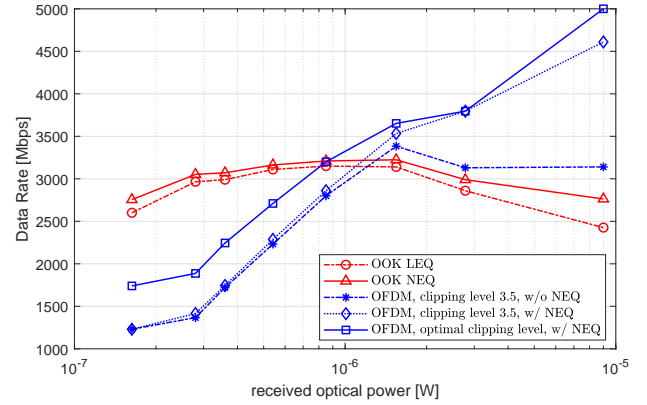


Fig. 7. The achievable data rate versus the received signal power for the considered modulation schemes. LEQ: linear equalization; NEQ: nonlinear equalization.

of nonlinear equalizer, with a normalized clipping level of 3, the achievable data rate for a BER target of 2×10^{-3} is 2.75 Gbps ; however, the corresponding data rate increases to 3.3 Gbps when the clipping level increases to 4.5. Fig. 5 also indicates that in order to achieve the highest achievable data rate, one can employ both the nonlinear equalizer and clipping optimization. The measured optimal clipping level versus the received optical power when nonlinear equalizer is employed is presented in Fig. 6. To achieve this result, a vector of clipping levels ranging from 2 to 4.5 with a step size of 0.5 is considered. For each received optical power, the clipping level which provides the highest achievable data rate is recorded. It is illustrated that with the increase of the received signal power, the optimal clipping level also increases to account for higher nonlinear effect.

Finally, Fig. 7 demonstrates the measured achievable data rate versus the received optical power for both OOK and OFDM with a BER target of 2×10^{-3} which is below the 7% forward error correction (FEC) limit, i.e., 3.8×10^{-3} . For OOK transmission, with the increase of the optical power, the increase and then decrease of the data rate can be observed. It is illustrated that employing the nonlinear equalizer can slightly improve the data rate. The measured highest achievable data rates of OOK are 3.15 Gbps and 3.22 Gbps when linear and nonlinear equalizers are employed, respectively, which are achieved at a received power of $0.85 \mu\text{W}$. This result is close to the record data rate of SPAD-based system with OOK, i.e., 3.6 Gbps , reported before [6]. To achieve a data rate of 3 Gbps , the required received optical power is $0.28 \mu\text{W}$ which corresponds to a sensitivity of -35 dBm . Considering that corresponding sensitivities of the state-of-the-art PIN PD and APD receivers are around -20 dBm and -30 dBm [16], the superiority of SPAD receiver over its counterparts in terms of the sensitivity is demonstrated.

On the other hand, when OFDM modulation is employed, in the absence of clipping optimization and nonlinear equalization, the change of the data rate with the increase of optical power is similar to that when OOK is employed. However, different from OOK transmission, employing the

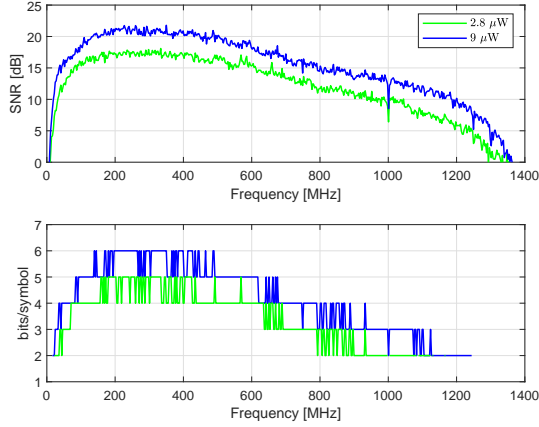


Fig. 8. The measured SNR and adaptively loaded bits for each subcarrier of OFDM when optimal clipping level and nonlinear equalizer are employed.

nonlinear equalization can significantly improve the data rate. For instance, when the received power is $9 \mu\text{W}$ and the clipping level is 3.5, the achievable data rate is 3.14 Gbps in the absence of nonlinear equalization; however, when the nonlinear equalizer is employed, this data rate rises to 4.6 Gbps. It is also presented in Fig. 7 that the clipping level optimization can further improve the data rate performance. By employing both nonlinear equalization and clipping level optimization, achievable data rates of 3.8 Gbps and 5 Gbps have been achieved when the received power is $2.8 \mu\text{W}$ and $9 \mu\text{W}$, respectively. The measured SNR and bit loading results for these two cases are shown in Fig. 8. It is illustrated that increasing the signal power from $2.8 \mu\text{W}$ to $9 \mu\text{W}$ can introduce around 3 dB SNR improvement over the whole considered spectrum range which strongly improves the spectrum efficiency.

The comparison of the achievable data rates of OOK and OFDM transmission presented in Fig. 7 further indicates that these two modulation schemes have contrasting optimal regimes of operation. When the received power is relatively low, i.e., below $0.85 \mu\text{W}$, due to the low dynamic range of the received optical signal, OOK can provide significantly higher data rates than OFDM which requires higher PAPR to achieve decent performance. However, OFDM in turn outperforms OOK in high power regime. Therefore, in practical implementation, OOK is preferable for applications with lower received power; whereas, for applications with higher received power, OFDM is a preferred choice. For links with a large dynamic range of channel gain, the adaptive switching between OOK and OFDM based on the instantaneous channel condition may be employed which can achieve the best data rate performance over a wide range of received power.

VI. CONCLUSION

In this work, the performance of the OWC system with commercial SPAD receiver is investigated. Two different modulation schemes are considered. To mitigate the effects of SPAD nonlinearity, Volterra series based nonlinear equalization is

employed. In addition, for OFDM transmission the optimization of normalized clipping level is further adopted. At a BER target of 2×10^{-3} , the achievable data rates of 3.22 Gbps and 5 Gbps have been experimentally demonstrated when OOK and OFDM are employed, respectively. The experimental results also illustrate that OOK and OFDM have contrasting operation regimes. For OWC systems with highly dynamic channels, the adaptive switching between these two modulation schemes may effectively improve the data rate over a wide range of received power.

VII. ACKNOWLEDGEMENTS

We gratefully acknowledge the financial support from EPSRC under grant EP/R023123/1 (ARROW).

REFERENCES

- [1] M. A. Khalighi and M. Uysal, "Survey on free space optical communication: A communication theory perspective," *IEEE Communications Surveys Tutorials*, vol. 16, no. 4, pp. 2231–2258, 2014.
- [2] H. Zimmermann, "APD and SPAD receivers : Invited paper," in *2019 15th International Conference on Telecommunications (ConTEL)*, 2019, pp. 1–5.
- [3] S. Huang and M. Safari, "Hybrid SPAD/PD receiver for reliable free-space optical communication," *IEEE Open Journal of the Communications Society*, vol. 1, pp. 1364–1373, 2020.
- [4] S. Huang, S. Patanwala, J. Kosman, R. K. Henderson, and M. Safari, "Optimal photon counting receiver for sub-dead-time signal transmission," *Journal of Lightwave Technology*, pp. 1–1, 2020.
- [5] Z. Ahmed, R. Singh, W. Ali, G. Faulkner, D. O'Brien, and S. Collins, "A SiPM-based VLC receiver for Gigabit communication using OOK modulation," *IEEE Photonics Technology Letters*, vol. 32, no. 6, pp. 317–320, 2020.
- [6] W. Matthews, Z. Ahmed, W. Ali, and S. Collins, "A 3.45 Gigabits/s sipm-based OOK VLC receiver," *IEEE Photonics Technology Letters*, vol. 33, no. 10, pp. 487–490, 2021.
- [7] ON Semiconductor, "J-SERIES SiPM: Silicon photomultiplier sensors, J-Series (SiPM)," Accessed: May 3, 2021. [Online]. Available: <https://www.onsemi.com/products/sensors/silicon-photomultipliers-sipm>.
- [8] W. Matthews, W. Ali, Z. Ahmed, G. Faulkner, and S. Collins, "Inter-symbol interference and silicon photomultiplier vlc receivers in ambient light," *IEEE Photonics Technology Letters*, vol. 33, no. 9, pp. 449–452, 2021.
- [9] A. Eisele, R. Henderson, B. Schmidtke, T. Funk, L. Grant, J. Richardson, and W. Freude, "185 MHz count rate 139 dB dynamic range single-photon avalanche diode with active quenching circuit in 130 nm CMOS technology," in *Proc. Int. Image Sensor Workshop*, 2011, pp. 278–280.
- [10] M. D. Soltani, A. A. Purwita, Z. Zeng, H. Haas, and M. Safari, "Modeling the random orientation of mobile devices: Measurement, analysis and lifi use case," *IEEE Transactions on Communications*, vol. 67, no. 3, pp. 2157–2172, 2019.
- [11] M. A. Khalighi, H. Akhoughyari, and S. Hranilovic, "Silicon-photomultiplier-based underwater wireless optical communication using pulse-amplitude modulation," *IEEE Journal of Oceanic Engineering*, pp. 1–11, 2019.
- [12] J. Kosman, O. Almer, T. A. Abbas, N. Dutton, R. Walker, S. Videv, K. Moore, H. Haas, and R. Henderson, "29.7 a 500Mb/s -46.1dBm CMOS SPAD receiver for laser diode visible-light communications," in *2019 IEEE International Solid-State Circuits Conference - (ISSCC)*, Feb 2019, pp. 468–470.
- [13] C. Chen, D. A. Basnayaka, and H. Haas, "Downlink performance of optical attocell networks," *Journal of Lightwave Technology*, vol. 34, no. 1, pp. 137–156, 2016.
- [14] R. Bian, I. Tavakkolnia, and H. Haas, "15.73 Gb/s visible light communication with off-the-shelf leds," *Journal of Lightwave Technology*, vol. 37, no. 10, pp. 2418–2424, 2019.
- [15] D. Tsonev, S. Sinanovic, and H. Haas, "Complete modeling of nonlinear distortion in ofdm-based optical wireless communication," *Journal of Lightwave Technology*, vol. 31, no. 18, pp. 3064–3076, 2013.
- [16] T. Jukić, B. Steindl, and H. Zimmermann, "400 μm diameter apd oec in0.35 μmbicmos," *IEEE Photonics Technology Letters*, vol. 28, no. 18, pp. 2004–2007, Sep. 2016.